N91-32648

FD-TD NUMERICAL SIMULATION OF AN ENTIRE LIGHTNING STRIKE ON THE C160 AIRCRAFT

J.C. Alliot*, J. Grando*, J.D. Muller* and X. Ferrières**

*Office National d'Etudes et de Recherches Aérospatiales,
B.P. 72, 92322 CHATILLON CEDEX, FRANCE

**SLX Informatique, 1 Place Charras, 92400 COURBEVOIE, FRANCE

ABSTRACT

Experimental transient electromagnetic fields measurements have been performed on a Transall C160 aircraft during in-flight lightning strikes. The data allow a test of the predictive capabilities of a three dimensional time-domain finite-difference code (ALICE) developed at ONERA in order to investigate lightning aircraft interactions. Using a transfer function technique in the 3D code it is shown that a bi-leader attached to an aircraft can be simulated by a linear model and so electromagnetic fields can be calculated everywhere on the vehicle. Comparison of experimental and numerical results have been made for several lightning strikes. Skin current density and electromagnetic fields distributions are discussed in detail.

1. INTRODUCTION

The electromagnetic pulses associated with a lightning threat can induce large charges and currents on the external skin of an aircraft in-flight that, in turn, couple into the interior of the vehicle where they can cause failures or temporary upsets in mission critical subsystems, if these subsystems are not sufficiently hardened. The recent introduction of advanced composite materials, sophisticated low level flights and mission critical electronics into aerospace vehicles has raised concerns that these may increase the vehicle's inherent susceptibility/vulnerability to transient electromagnetic fields.

Because of this concern, DRET (Direction des Recherches, Etudes et Techniques) has been sponsoring, for several years, a research program to investigate aircraft interaction with direct lightning strikes and to develop analytical and numerical tools necessary for a theoretical determination or prediction of lightning electromagnetic interactions with a vehicle.

The most recent in-flight program was conducted in France with an instrumented C160 Transall aircraft [1].

The data obtained allowed a test of the predictive capabilities of a three-dimensional finite-difference computer code set up at ONERA in order to calculate charge and current distributions on the external skin of an in-flight vehicle struck by lightning.

Magnetic field coupling through a carbon composite panel located on the fuselage has also been studied [2]. The experimental and numerical results are compared for several strikes.

2. IN-FLIGHT INSTRUMENTATION DESCRIPTION

During Summer 1988, ONERA has performed a complete airborne lightning characterization program, including sensors design, instrumentation lay out, extensive ground test of the whole aircraft set in a coaxial return path and in-flight measurements. The sensors were implemented on the aircraft as shown in figure 1. Four resistive current shunts (I) were mounted on the aircraft. One was fixed to the nose-boom, two were fixed to the wing tips and one was located at the base of the tail-boom. Two derivative current sensors (I-Dot) were also installed in the middle of the front and tail-booms. Seven locations were instrumented with electromagnetic sensors for E, H, E-Dot, H-Dot external fields measurements (noted EH1 to EH7 in figure 1). An internal magnetic field measurement has been achieved at the center of the fuselage, behind a carbon composite panel located on the left side of the aircraft. Seven video cameras were used to record the scene all around the aircraft. One of them was a 200 frames/second camera located under the right wing. A more detailed description of the instrumentation and of the sensors characteristics is given in [1].

3. NUMERICAL SIMULATION METHOD

The numerical code "ALICE" employed in this study can take into account lightning electromagnetic interactions with a vehicle (nearby and direct strikes, electromagnetic coupling through lossy structures, coupling through resistive and isotropic joints, ...).

3.1. FINITE-DIFFERENCE TIME-DOMAIN METHOD

The code is based on an explicite Finite-Difference Time-Domain (FD-TD) algorithm developed by K.S. Yee [3] in cartesian coordinates. The goal of the FD-TD method is to model the propagation of an electromagnetic wave into a volume of space containing a dielectric or conducting structure. The procedure produces a finite difference approximation to the solution of Maxwell's differential curl equations implemented on rectangular cross section-unit-cell space lattice.

The differential time domain form of Maxwell's equations in an isotropic medium is:

$$\nabla \times \mathbf{E} = -\frac{\partial \mathbf{B}}{\partial t} \tag{1}$$

$$\nabla \times \mathbf{H} = \mathbf{J} + \frac{\partial \mathbf{D}}{\partial t} \tag{2}$$

with: $\mathbf{B} = \mu_o \mathbf{H}$; $\mathbf{D} = \varepsilon_o \mathbf{E}$.

These equations are written in the code in a finite difference form. For a parallelepipedic cell space lattice, this procedure involves positioning the components of E and H about a unit cell of the lattice, as shown in figure 2,

and evaluating E and H at alternate half time steps. In this manner, centered difference expressions can be used for both the space and time derivatives to attain second-order accuracy in the space and time increments. The size of the unit cell determines the time step Δt which, for numerical stability condition, must satisfy the criterion:

$$\Delta t^2 \leq \frac{\varepsilon_o \mu_o}{1/\Delta x^2 + 1/\Delta y^2 + 1/\Delta z^2} \tag{3}$$

where Δx, Δy and Δz are the dimensions of a cell (figure 2).

3.2. LATTICE TRUNCATION CONDITIONS

To minimize computer storage, the lattice must be truncated as close as possible to the modelled structure. However, care must be exercised because this condition must not cause excessive spurious reflection of waves scattered outward by the structure.
The field components at the lattice truncation planes must be computed using an auxiliary radiative truncation condition. The method used in "ALICE" is achieved by using highly absorbing boundary conditions to simulate free space. This approximation is successful when the lattice is at least twice the largest vehicle dimension in each direction of space.

3.3. THIN WIRE FORMALISM

FD-TD codes cannot resolve coupling to wires of diameters less than a mesh size unless special features are added. The thin-strut formalism developed by R. Holland [4] allows such resolution and has been introduced in "ALICE". On a wire segment parallel to the x-axis (λ, μ coordinate location of the wire - figure 2). The current I and the charge Q per unit length are calculated by finite differencing the two following equations:

$$\frac{\partial Q}{\partial t} = - \frac{\partial I}{\partial x} \tag{4}$$

$$\frac{\partial I}{\partial t} = - C^2 \frac{\partial Q}{\partial x} + \frac{\langle E_x \rangle}{L_x} \tag{5}$$

where

C is the light velocity.
$\langle E_x \rangle$ is the electric field component averaged over the cross section of the cell surrounding the wire.
L_x is the in-cell inductance, the inductance per unit length a thin wire would have with respect to an enclosing conductor half a mesh removed.

Thus, a cell with a wire running through it requires eight quantities (six fields components, the current I and the charge density Q) to be advanced each program cycle.

3.4. TRANSALL AIRCRAFT MODELLING

The Transall aircraft was modelled using three-dimensional rectangular cells having dimensions of Δx = 45 cm, Δy = 90 cm and Δz = 45 cm that were part of a total cell space of 121 x 70 x 79 cells. The relatively small cell size allows a reasonable condition of the aircraft geometry to be made as figure 3 reveals. The time step Δt employed is found from the condition (3) and has been chosen equal to 0.9 ns. For the external fields calculations a uniform mesh has been used inside a box that just encloses the modelled aircraft-extremities and slowly varying around it (adjacent cells differed in size by 20%). For the internal fields calculations, a varying mesh has been chosen on the aircraft in order to properly take into account the right composite door dimensions and a second one in space around the aircraft as in the previous meshing.
The metallic parts of the vehicle are modelled by the necessary condition:

$$\vec{n} \wedge \vec{E} = 0 \qquad (6)$$

on the structure, $\vec{n}$ is a unit vector perpendicular to the surface.

The connecting lightning channels are modelled using thin wire formalism describe in § 3.3.
A test of the predictive capabilities of the computer code "ALICE" has been performed, several years ago, by comparing experimental and numerical results obtained on an aircraft mock-up [5].

4. COMPARISON OF NUMERICAL PREDICTIONS AND IN-FLIGHT MEASUREMENTS

We give here the comparison of experimental and theoretical results obtained for a nose-wing lightning strike obtained during the 1988 in-flight experiment. For this event electromagnetic signatures on the sensors and photographic evidence from the on-board video cameras indicated that the aircraft initiated a bi-leader mechanism. The sequence of the phenomena is the following (figure 4a):

- at the beginning (between A and B) the aircraft is immersed in an ambiant electrostatic field,
- at the nose-boom, the electric field is high enough to initiate a positive leader which propagates towards ground (between B and C),
- at the right wing tip, a negative leader is initiated and propagates, by steps, towards the rear part of the fuselage (between C and E). The direction of propagation is parallel to the fuselage as shown in figure 3. It is to be noticed that the negative leader propagation generates current pulses which are superimposed on a slowly varying current component (figure 4b).

The numerical simulation of this event has been achieved for the phenomena occuring between points C and E in figure 4a. During this phase, the positive leader could be considered as having an infinite length and the negative leader could be considered as having a 30 m characteristic length corresponding to its first step [6].

The numerical calculations have been undertaken in two steps using a frequency domain transfer function technique.

4.1. ELEMENTARY PULSES MODELLING

The principle of the transfer function method is the following:

a) We assume the lightning aircraft interaction is a linear mechanism. So, for a given geometry of the vehicle attached to lightning channels (as shown in figure 3) one can put, in the 3-D code, a current generator in place of the negative leader tip and which injects a known current pulse $I_o(t)$ towards the aircraft. In one point p_o of the vehicle (taken as a reference point) a magnetic field response $H_o(t)$ can be calculated and using a FFT of $H_o(t)$ and $I_o(t)$ one can then determine (in the frequency domain) a transfer function $T(F)$ between these two points:

$$T(F) = H_o(F)/I_o(F) \tag{7}$$

where F is the frequency and $H_o(F)$, $I_o(F)$ are the FFT of $H_o(t)$, $I_o(t)$ respectively.
We generally use a standard sine-squared pulse for $I_o(t)$:

$$I_o(t) = I_M \sin^2(\pi t/2\tau) \tag{8}$$

where τ is chosen in function of the frequency content of the in-flight measured responses.

b) If we consider the response $H_3(t)$ which has been obtained, at the same point P_o on the aircraft, during in-flight experiment, its FFT $H_3(F)$ allows the calculation, in the frequency domain, of an equivalent current generator I(F) located at the negative leader extremity and defined by:

$$I(F) = H_3(F)/T(F) \tag{9}$$

and in time domain:

$$I(t) = IFT\,[I(F)] \tag{10}$$

c) This current waveform I(t), simulating the negative leader mechanism, is introduced in the 3-D code and then the temporal responses at every instrumented points on the aircraft (figure 1) can be computed and compared to experimental data.
This technique is illustrated in figure 5 to 8, for the measurement current pulse noted "pulse n°7" in figure 4b. The pulse noted "pulse n°2" has been studied previously [5] using the same technique.

Figure 5 represents the comparison between magnetic field pulses measured and calculated on the left side (curves a), on the right side (curves b) and on the top (curves c) of the forward fuselage.

Figure 6 represents the comparison between magnetic field pulses measured and calculated inside the fuselage, behind the carbon composite door.

Figure 7 represents the comparison between electric field pulses measured and calculated on the top of the forward fuselage.

Figure 8 represents the comparison between the current pulses measured and calculated on the right wing tip (curves a) and on the nose boom (curves b). The magnetic field H_3 measured on the top of the fuselage has been used as reference to compute the transfer function T(F). The comparisons show a good agreement between measured and calculated waveforms at different locations on the aircraft, the magnitude discrepancy is better than 3 dB for all the fields and currents.

4.2. PULSE SERIES MODELLING

Knowing the entire strike response of a sensor in one point on the aircraft, we can calculate the responses everywhere on the aircraft using the transfer function technique described previously.

In the phase a) of § 4.1 we can calculate the transient response $H_o(t)$ at the reference point P_o but also the transient responses $H_1(t)$ at different points P_1 of interest on the aircraft.
We can then determine (in the frequency domain) the transfer functions $T_1(F)$ beetween the points P_1 and the reference point P_o, such as:

$$T_1(F) = H_1(F)/H_o(F) \qquad (11)$$

where $H_1(F)$ and $H_o(F)$ are the FFT of $H_1(t)$ and $H_o(t)$ respectively.

If we consider the pulses series $H_3(t)$ (figure 9) which has been measured during in-flight experiment at point P_o on the top of the front fuselage (figure 1), its FFT $H_3(F)$ allows the calculation, in the frequency domain, of the responses $H_1(F)$ at each point P_1:

$$H_1(F) = T_1(F).H_3(F) \qquad (12)$$

This technique is illustrated in figures 10 to 12.

Figure 10 represents the comparison between the magnetic fields measured (curve a) and calculated (curve b) on the left side of the forward fuselage.

Figure 11 represents the comparison between the magnetic fields measured (curve a) and calculated (curve b) inside the fuselage, behind the carbon composite door. The pulses of the measured field (curve a) are superimposed on a CW component due to an induced effect on the sensor of the aircraft power supply.

Figure 12 represents the comparison between the currents measured (curve a) and calculated (curve b) at the right wing tip. As explained in § 4, the measured current pulses are superimposed on a slowly varying current component. This low frequency component has not been measured by the magnetic field sensor H_3 (cut-off frequency of 100 Hz - figure 9) and so can not be

calculated (figure 12b) using relation (12).

5. CONCLUSION

The goal of this paper is to present a 3-D FD-TD computer code developed at ONERA to model ligthning interaction with an aircraft. The predictive capabilities of the code have been quantified, a few years ago, by comparing experimental and computed results obtained on an aircraft mock-up and on an helicopter carbon composite fuselage.

We show in this paper that the code may be a powerful tool to analyse in-flight data. Using a transfer function technique, it has been shown that a bi-leader attached to an aircraft can be simulated by a linear model and so E.M. fields can be calculated everywhere on the vehicle.

Furthermore, knowing the entire strike response of a sensor in one point on the aircraft, we can calculate the responses everywhere on the aircraft.

REFERENCES

[1] Moreau, J.P.; Jouan, J.Y.; Issac, F.: Transall 88 characterization program. Proceedings of ICOLSE Conf., Bath (UK), (Sept. 26-28, 1989).

[2] Alliot, J.C.; Grando, J.; Issac, F; Ferrières, X.: FD-TD calculation with composite materials. Application to C160 aircraft measurements. International Aerospace and Ground Conference on Lightning and Static Electricity, Cocoa Beach, Florida (USA), (April 16-19 1991).

[3] Yee, K.S.: Numerical solution of initial boundary value problems involving Maxwell's equations in isotropic media. IEEE Trans. Ant. and Prop., Vol. AP 14, 302-307 (May 1966).

[4] Holland R.; Simpson L.: Finite-difference analysis of EMP coupling to thin struts and wires. IEEE Trans. on EMC, Vol. EMC 33, No 2, 88-97 (May 1981).

[5] Grando J.; Labaune G.; Alliot J.C.; Issac F.: Comparison of experimental and numerical results for transient electromagnetic fields induced on the C160 aircraft by current injection techniques. ICOLSE 1989, Bath (UK) (Sept.26-28 1989).

[6] Labaune G.; Richard P.; Bondiou A.: Electromagnetic properties of a lightning channel formation and propagation. Electro-magnetics, Vol. 7, No 3-4, 361-393 (1987).

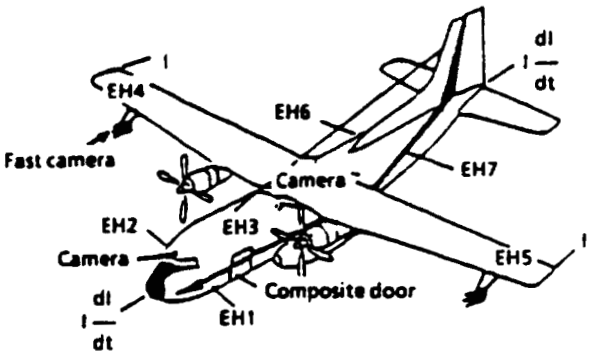

Fig. 1 : Sensors locations on the aircraft.

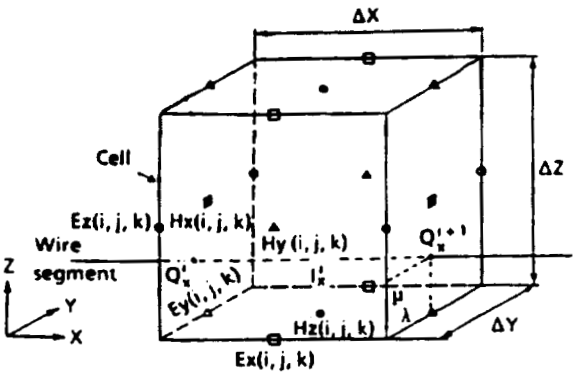

Fig. 2 : Location of I, Q and the six field-evaluation points in a unit cell.

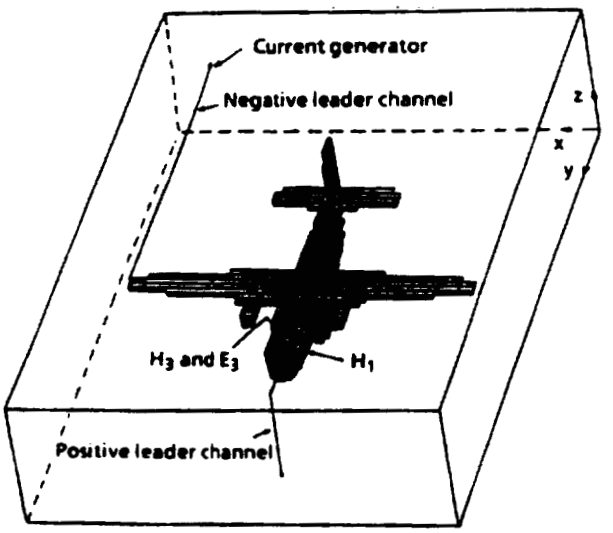

Fig. 3 : 3-D model of the Transall aircraft attached to a lightning channel.

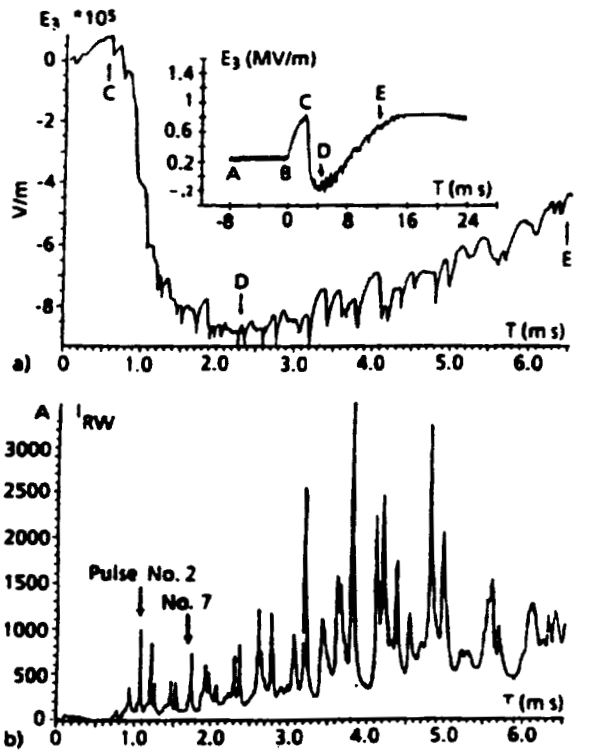

Fig. 4 : Typical experimental signatures of a bi-leader mechanism.

a) Electric field variations on two time scales.
b) Current waveform on the right wing-boom.

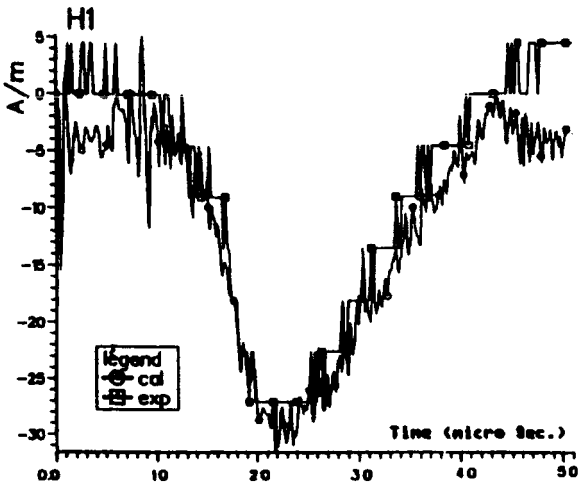

a) On the left side of the forward fuselage.

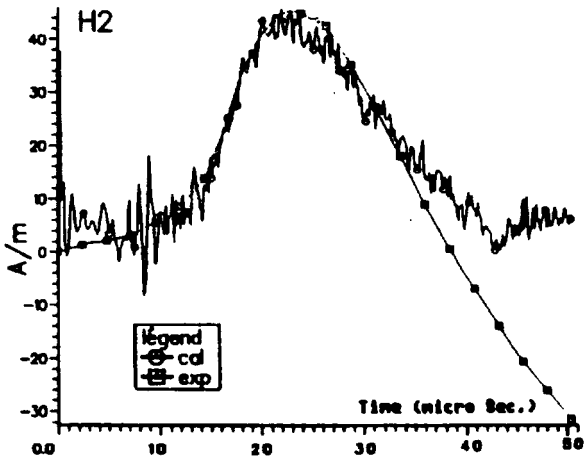

b) On the right side of the forward fuselage.

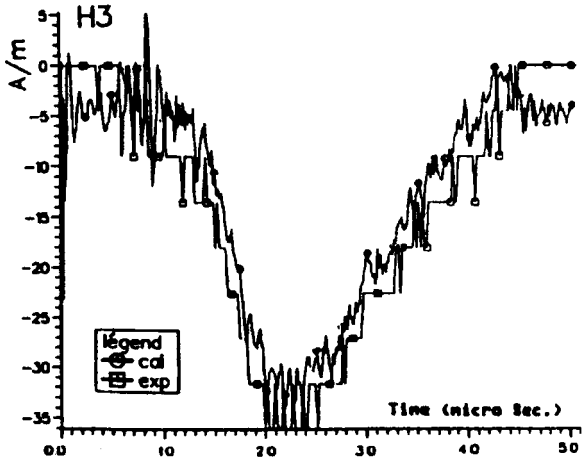

c) On the top of the forward fuselage.

Fig. 5 : Comparison of measured and calculated magnetic field pulses:

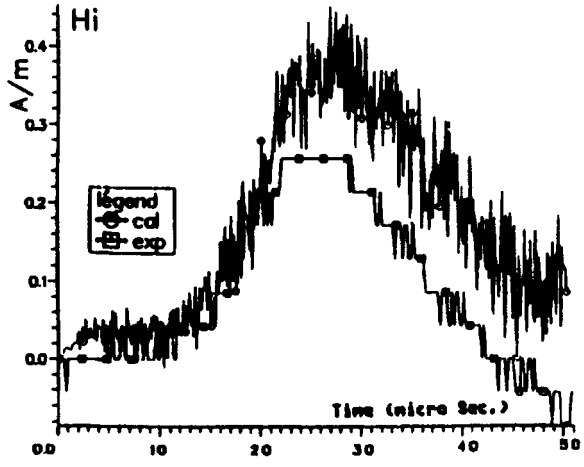

Fig. 6 : Comparison of the magnetic field pulses measured and calculated inside the fuselage behind the carbon composite door.

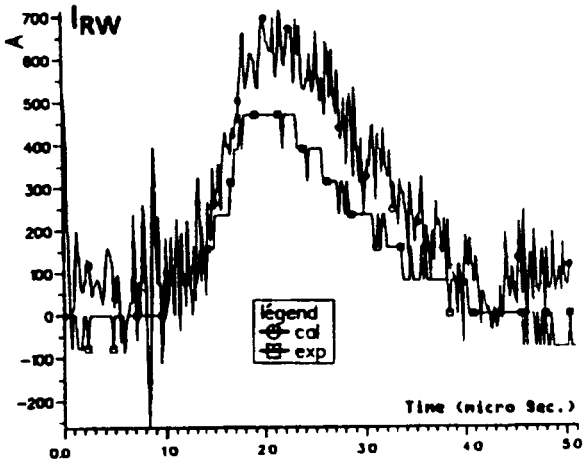

a) At the right wing tip.

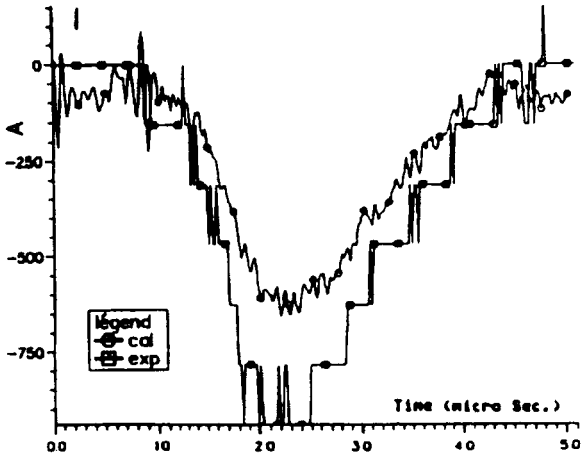

b) On the nose boom.

Fig. 8 : Comparison of measured and calculated current pulses:

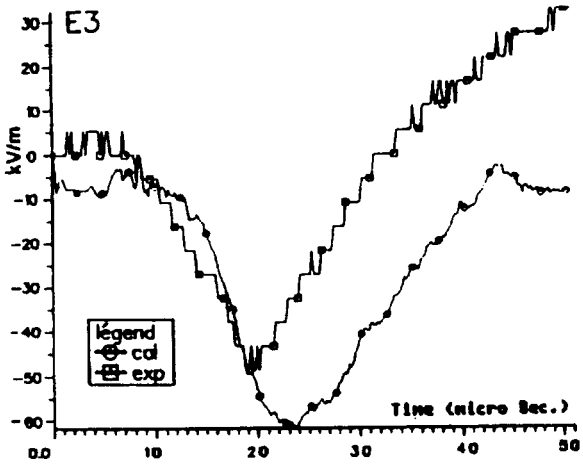

Fig. 7 : Comparison of the electric field pulses measured and calculated on the top of the forward fuselage.

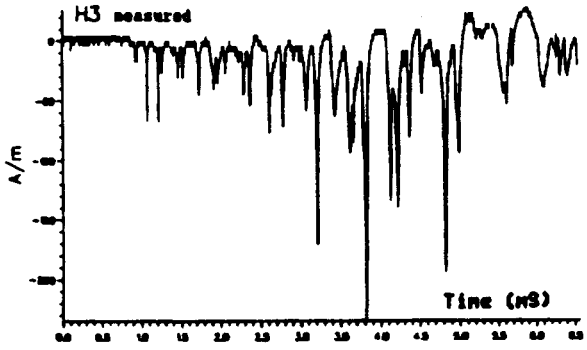

Fig. 9 : Magnetic field measured on the top of the forward fuselage.

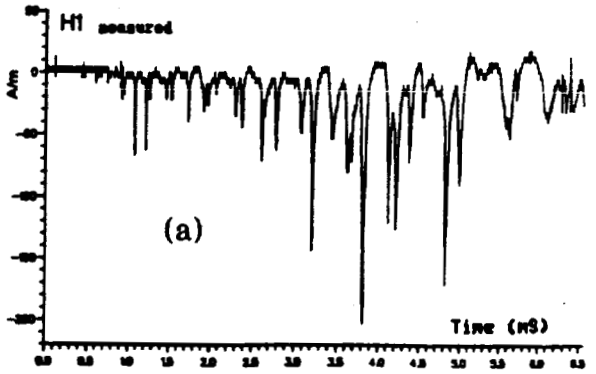

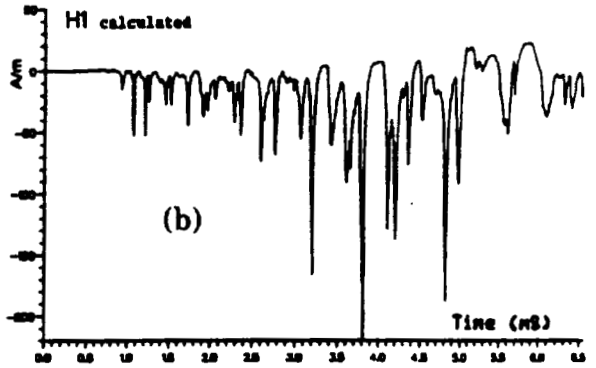

Fig. 10 : Comparison of the magnetic fields measured (a) and calculated (b) on the left side of the forward fuselage.

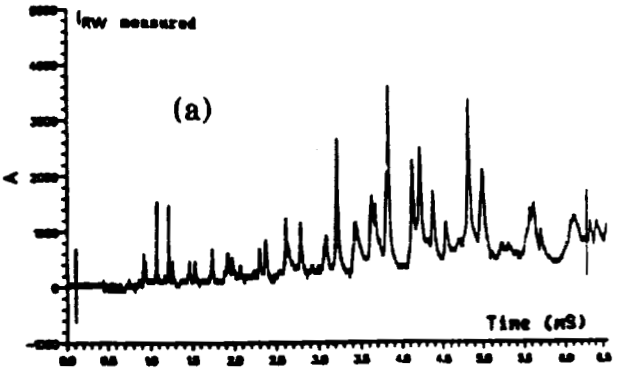

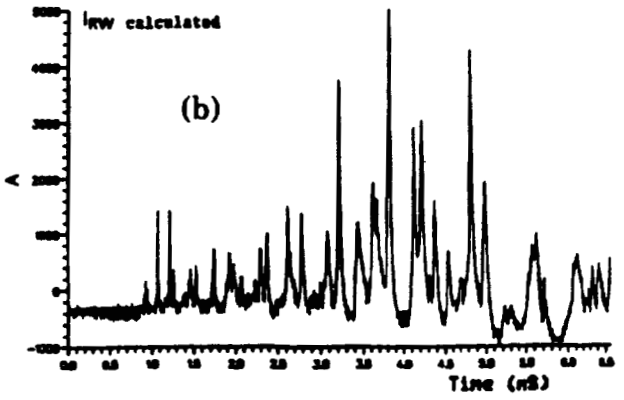

Fig. 12 : Comparison of the currents measured (a) and calculated (b) at the right wing tip.

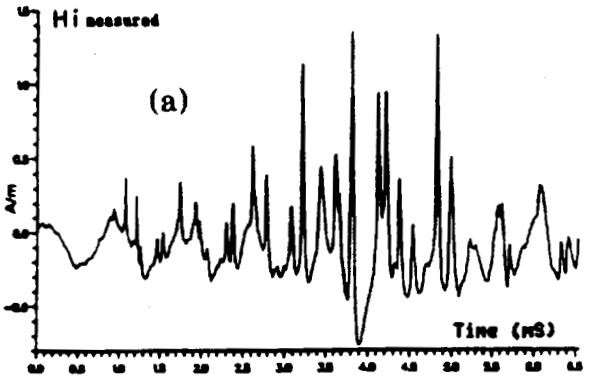

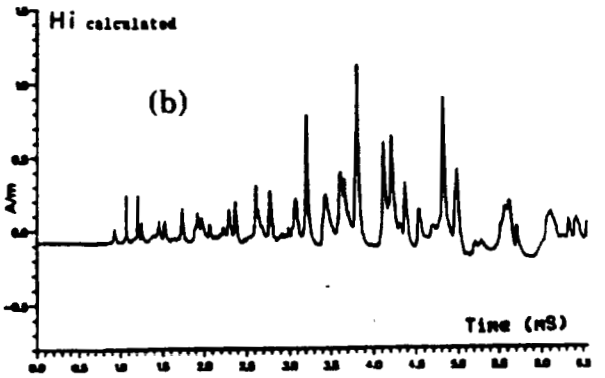

Fig. 11 : Comparison of the magnetic fields measured (a) and calculated (b) inside the fuselage behind the carbon composite door.